

Region-to-Region: Enhancing Generative Image Harmonization with Adaptive Regional Injection

Zhiqiu Zhang¹, Dongqi Fan¹, Mingjie Wang², Qiang Tang³, Jian Yang¹, Zili Yi¹

¹Nanjing University

²Zhejiang Sci-Tech University

³Electronic Arts

zhiqiuzhang@smail.nju.edu.cn

Abstract

The goal of image harmonization is to adjust the foreground in a composite image to achieve visual consistency with the background. Recently, latent diffusion model (LDM) are applied for harmonization, achieving remarkable results. However, LDM-based harmonization faces challenges in detail preservation and limited harmonization ability. Additionally, current synthetic datasets rely on color transfer, which lacks local variations and fails to capture complex real-world lighting conditions. To enhance harmonization capabilities, we propose the *Region-to-Region* transformation. By injecting information from appropriate regions into the foreground, this approach preserves original details while achieving image harmonization or, conversely, generating new composite data. From this perspective, We propose a novel model *R2R*. Specifically, we design *Clear-VAE* to preserve high-frequency details in the foreground using Adaptive Filter while eliminating disharmonious elements. To further enhance harmonization, we introduce the *Harmony Controller* with Mask-aware Adaptive Channel Attention (MACA), which dynamically adjusts the foreground based on the channel importance of both foreground and background regions. To address the limitation of existing datasets, we propose *Random Poisson Blending*, which transfers color and lighting information from a suitable region to the foreground, thereby generating more diverse and challenging synthetic images. Using this method, we construct a new synthetic dataset, *RPHarmony*. Experiments demonstrate the superiority of our method over other methods in both quantitative metrics and visual harmony. Moreover, our dataset helps the model generate more realistic images in real examples. Our code, dataset, and model weights have all been released for open access.

Code —

https://github.com/anonymity-111/Region_to_Region

Introduction

Compositing images with inconsistent conditions creates unrealistic results. Image harmonization refines the foreground to align with the background’s color and lighting, ensuring a more natural blend.

Numerous methods have been proposed for the image harmonization task. Traditionally, this problem has

been approached either through image gradient-based techniques (Pérez, Gangnet, and Blake 2003; Jia et al. 2006) for seamless blending or from a statistical perspective (Cohen-Or et al. 2006; Pitie, Kokaram, and Dahyot 2005). With the advent of deep learning, learning-based methods trained on large-scale datasets have achieved significant advancements in this field (Cong et al. 2020; Ling et al. 2021; Chen et al. 2023a; Xue et al. 2022). Recently, diffusion model (Ho, Jain, and Abbeel 2020), particularly latent diffusion model (LDM) (Rombach et al. 2022), have become the mainstream paradigm for image generation. Some works have applied LDM to address the image harmonization task, leveraging the rich prior knowledge of diffusion models (Li et al. 2023; Chen et al. 2023b; Zhou, Feng, and Wang 2024; Zhou et al. 2024; Hachnouchi et al. 2023).

While recent advancements have led to significant progress in the qualitative metrics of datasets, state-of-the-art models, including LDM-based methods, still struggle with real composite images. This shortcoming arises from both the model architecture and the limitations of current training datasets.

From a model perspective, applying LDM to image harmonization presents two key challenges. First, the VAE encoding process can result in a loss of fine details, a concern also noted in (Yu et al. 2024; Zhou, Feng, and Wang 2024; Zhou et al. 2024). While some methods attempt to address this, they often preserve details at the expense of introducing disharmonious elements from the original foreground. Second, the vanilla LDM, designed for general image generation, has inherent limitations in harmonization capabilities. Resolving these two challenges will further unleash the potential of LDM in advancing image harmonization.

The limitations of existing datasets also compound this issue. Mainstream datasets, such as iHarmony4 (Cong et al. 2020), are typically generated using the color transfer method (Tsai et al. 2017). This technique modifies the foreground of a real image by referencing semantically similar objects from another image. However, this approach primarily applies global adjustments, neglecting local variations in color and lighting (Ren et al. 2024). As a result, these synthetic images do not fully represent the complexity of real-world lighting conditions, thereby hindering progress in image harmonization.

To address model and dataset limitations, we propose

a **Region-to-Region** transformation approach. Specifically, transformation is achieved by injecting information from appropriate regions—background, composite foreground, or a specific area from a reference image—into the foreground region.

Compared to global color-to-color or local pixel-to-pixel adjustments (Cong et al. 2022), our transformation operates at an intermediate scale such as the region (a group of pixels), balancing global and local information.

From this perspective, we design a novel model, **R2R**. First, we propose **Clear-VAE**, an improved VAE that incorporates skip connection with Adaptive Filter in each layer to restore high-frequency details from the composite foreground. During training, we introduce contrastive regulation loss (Hang et al. 2022) to remove disharmonious elements in high-frequency details. Moreover, we introduce the **Harmony Controller**, a ControlNet-like structure (Zhang, Rao, and Agrawala 2023; Chen et al. 2024), to enhance the U-Net for generation. Within each block, we integrate Mask-aware Adaptive Channel Attention (**MACA**), which adaptively refines foreground features based on the channel importance of both foreground and background regions, guided by the mask.

Meanwhile, we propose **Random Poisson Blending**, a data synthesis technique motivated by the Region-to-Region transformation paradigm, for constructing a more realistic dataset. Our approach uses Poisson Blending (Pérez, Gangnet, and Blake 2003) to directly apply background information from random regions in a reference image to modify the foreground of a real image. Using this method, we introduce a new dataset, **RPHarmony**, consisting of 12,787 training images and 1,422 test images. With a more diverse and challenging set of composite images, RPHarmony enables models to achieve more effective image harmonization in real-world scenarios after fine-tuning (Fig. 4).

Our contributions can be summarized as follows:

- We introduce Region-to-Region transformation for harmonization. From this perspective, we introduce R2R, a novel model that enhances Generative Image Harmonization through regional injection.
- We propose Random Poisson Blending, a Region-to-Region transformation method, to generate composite images and create a new dataset, RPHarmony. Compared to iHarmony4, our dataset provides more realistic and complex composite images, bridging the gap to real-world scenarios.
- Our model achieves new state-of-the-art performance on the iHarmony4 dataset, with a 0.28dB improvement in PSNR and over 10% reduction in MSE. Additionally, results on real-world composite images indicate that both our R2R model and RPHarmony dataset significantly contribute to improving the generalization capability of harmonization models.

Related Work

Diffusion Model

Diffusion model (Ho, Jain, and Abbeel 2020; Song, Meng, and Ermon 2022) has shown strong capabilities in realistic

image generation. Latent Diffusion Models (LDMs) (Romach et al. 2022) improve efficiency by operating in the latent space. To enable controllable generation, ControlNet (Zhang, Rao, and Agrawala 2023) introduces an auxiliary encoder to inject image conditions into the diffusion process, and has been widely used in image-to-image translation (Chen et al. 2024; Li et al. 2024).

Image Harmonization

Image harmonization aims to adjust the foreground to be visually consistent with the background in terms of color, lighting, and other low-level cues (Niu et al. 2024). Traditional methods rely on gradient-based (Pérez, Gangnet, and Blake 2003; Jia et al. 2006) and statistical approaches (Cohen-Or et al. 2006; Pitie, Kokaram, and Dahyot 2005).

Recent advances are dominated by deep learning techniques. Most learning-based methods adopt U-Net-style encoder-decoder frameworks with task-specific modules (Cong et al. 2020; Ling et al. 2021; Chen et al. 2023a). Several works explore full-resolution harmonization by combining low- and high-resolution branches using learned transformations (Xue et al. 2022; Guerreiro, Nakazawa, and Stenger 2023; Meng et al. 2024). Recently, diffusion models have been introduced for harmonization. Li et al. (Li et al. 2023) employ ControlNet with HSV/HSL color transfer, while Chen et al. (Chen et al. 2023b) propose a zero-shot diffusion-VLM pipeline. Zhou et al. (Zhou, Feng, and Wang 2024; Zhou et al. 2024) address latent distortion with a refined stage or Harmony-VAE, achieving state-of-the-art (SOTA) results.

Image Harmonization Dataset

Existing dataset construction methods can be grouped into four categories: (1) Capture-based: Collecting real images of the same foreground under different backgrounds (e.g., GMSDataset (Song et al. 2020), Hday2night (Cong et al. 2020; Laffont et al. 2014)); (2) Manual adjustment: Using professional adjustments of foregrounds to generate variants (e.g., HAdobe5k (Cong et al. 2020), RealHM (Jiang et al. 2021)). These two methods are often time-consuming and labor-intensive. (3) Rendering-based: Placing 3D models in virtual scenes to simulate realistic lighting and shadows (e.g., RdHarmony (Cao et al. 2022), IllumHarmony (Hu et al. 2024)), though domain gaps remain a challenge; (4) Synthetic foreground generation: Creating disharmonious composites by manipulating foreground appearance, with color transfer being a representative approach (e.g., HFlickr and HCOCO in iHarmony4 (Cong et al. 2020)). Our proposed method, Random Poisson Blending falls into the category (4), but introduces richer and more realistic variations in lighting and color, which help improve model generalization to real-harmonization images.

Method

Overall Model Architecture and Data Flow

Our model is based on the LDM, which consists of two parts: Variational AutoEncoder (VAE) and diffusion network (i.e.

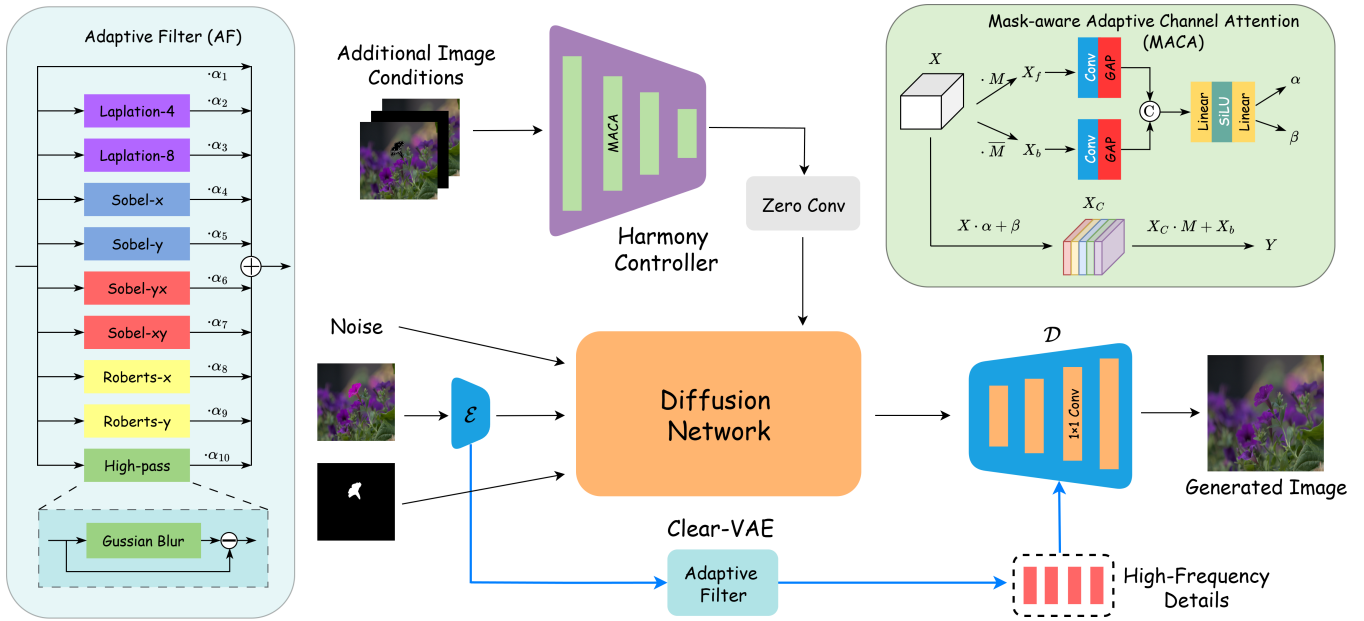


Figure 1. **Overview of our model structure.** The R2R model consists of three components: the Clear-VAE, which encodes initial composite images and decodes predicted images while using the Adaptive Filter to extract high-frequency details for appearance consistency; the Harmony Controller with MACA, which takes Additional Image Conditions as input to extract and form image guidance conditions; and the Diffusion Network, which performs image harmonization in latent space with the injection from Controller.

U-Net). The VAE includes an Encoder \mathcal{E} and a Decoder \mathcal{D} . The Encoder maps an image I to the latent space, $z = \mathcal{E}(I)$, while the Decoder reconstructs the image from the latent space, $\hat{I} = \mathcal{D}(z)$. In the first stage, the VAE is trained independently. Then, VAE is locked and the diffusion U-Net is trained in the latent space.

During the inference phase, a pure noise z_T is first sampled from a Gaussian distribution. Then, the diffusion U-Net iteratively predicts the noise at each time step t and denoises to obtain z'_0 . Finally, the VAE decoder \mathcal{D} projects back to the pixel space to reconstruct the image.

Given the foreground image I_f , the background image I_b , and the foreground mask M , the composite image I_c can be defined as: $I_c = M \times I_f + (1 - M) \times I_b$. In our approach, I_c is encoded into latent space, then the harmonization process is carried out in the latent space. Finally, the denoising result is decoded back into pixel space as the image harmonization output.

Compared to LDM, our model has two improvements. We replace the original VAE with Clear-VAE, incorporate the Harmony Controller with MACA, and perform fine-tuning. The following will provide a detailed explanation.

Clear-VAE

During VAE encoding process, detail information is lost, leading to a decline in the quality of generated images with unclear details. Therefore, we need to restore these details from the composite images. However, directly incorporating content from the original foreground (Yu et al. 2024; Zhou, Feng, and Wang 2024; Zhou et al. 2024), while preserving

details, also introduces disharmonious elements that negatively impact the generated images.

We propose a new VAE architecture, named **Clear-VAE**. Preserving high-frequency information in the foreground region helps maintain content details while remaining unaffected by disharmonious factors. We use **Adaptive Filter** (AF) to extract high-frequency details from skip-connect features in each layer, and then apply zero-initialized 1×1 convolutions to merge them with features in the decoder. As shown in Fig. 1, AF offers a wide range of filters with adaptive learnable parameters α . Each filter in the AF has its own advantages and disadvantages. Thus, we use the learnable parameters to adaptively combine them together, extracting more types of useful information. Furthermore, the AF can be reparameterized as one 3×3 and one high-pass filter after training to achieve lightweight. Clear-VAE is trained independently with the contrastive regularization loss (Eq. (4)).

Harmony Controller with MACA

To inject additional image conditions (such as masks, composite images, Canny edges, etc.) in LDM, we add a ControlNet-style (Zhang, Rao, and Agrawala 2023) adaptive encoder as the Harmony Controller (Fig. 1). As a result, more image information can be adaptively injected into the output, while maintaining the stability of the diffusion network.

Self-attention and cross-attention are widely used in LDM to model the importance relationships between pixels and between pixels and text condition (Rombach et al. 2022). However, compared to pixel information, channel informa-

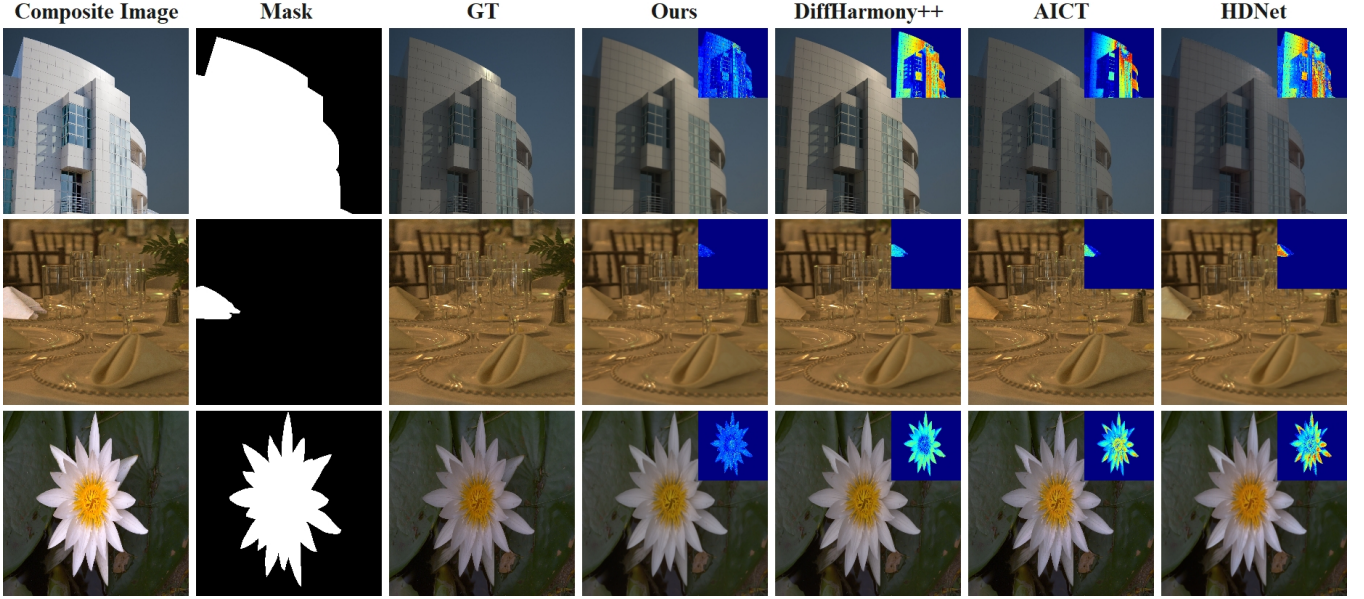


Figure 2. **Qualitative comparison results and error maps on the testing dataset of iHarmony4 (Cong et al. 2020).** The error maps are computed based on absolute error.

tion is more suitable for capturing the style of the foreground region. And pixel-level adaptation is unsuitable for low-level color and texture features (Chen et al. 2023a). Nevertheless, we observe that previous works learn the channel importance either through global pooling applied to the entire feature map (Woo et al. 2018; Cun and Pun 2020) or by separately processing the foreground and background regions (Chen et al. 2023a), lacking cross-integration of channel information between them. Based on these observations, we propose a new module called **Mask-aware Adaptive Channel Attention (MACA)**. This module (Fig. 1) adaptively adjusts the importance of channels in the feature map based on the channel information of both the foreground and background.

For the feature map $X \in R^{H \times W \times C}$, we first use a mask $M \in R^{H \times W \times 1}$ (and reverse mask $\bar{M} = 1 - M$) to obtain the foreground feature map X_f (and the background feature map X_b), i.e., $X_f = X \cdot M$, $X_b = X \cdot \bar{M}$.

These two feature maps are then processed through convolution and Global Average Pooling (GAP) to obtain the global channel information $C_f \in R^{1 \times 1 \times C}$ and $C_b \in R^{1 \times 1 \times C}$, respectively. The global channel information C_f and C_b are concatenated and passed through an MLP, which regresses to obtain the scale factor $\alpha \in R^{1 \times 1 \times C}$ and the shift factor $\beta \in R^{1 \times 1 \times C}$. The feature map X is then adjusted using the following formula to obtain X_c :

$$X_c = X \cdot \alpha + \beta \quad (1)$$

Similarly, we use the mask M to ensure that the adjusted features only inject to the foreground part. Therefore, the output Y of MACA is represented as:

$$Y = X_c \cdot M + X_b \quad (2)$$

The encoder architecture in LDM (same as the controller) can be divided into four blocks based on the feature map size (Zhang, Rao, and Agrawala 2023). At the end of each block, we insert MACA to integrate the channel importance information at that scale and adjust the feature map accordingly. MACA adjusts low-level features such as style, color, and brightness by enhancing or suppressing specific channels.

Training and Loss Function

Training of Clear-VAE Clear-VAE is trained separately following (Rombach et al. 2022). We fix the encoder and fine-tune the AF and decoder. The supervised training objective is to reconstruct real images. During training, the encoder encodes both the ground truth I and composite image I_c , resulting in z and z_c . The skip-connect features s_c from encoding composite images, after high-frequency information extraction via AF, is added to decoding z , obtaining the reconstructed images $\hat{I} = \mathcal{D}(z, \text{AF}(s))$. In the inference stage, the skip-connect features extracted from the composite image is used to guide the reconstruction of the output of DM.

To measure the difference between the reconstructed image and the ground truth (GT), we use the MSE Loss as the base loss function.

$$\mathcal{L}_{rec} = \|I - \hat{I}\|_2^2 \quad (3)$$

Using skip-connect features from composite images during the decoding phase can help preserve fine details. However, it also carries the risk of introducing disharmonious information, which may negatively impact the generated foreground. To address this, we also introduce **contrastive regularization loss** \mathcal{L}_{cr} , aiming to ensure that the reconstructed image is not only close to the positive samples (real images)

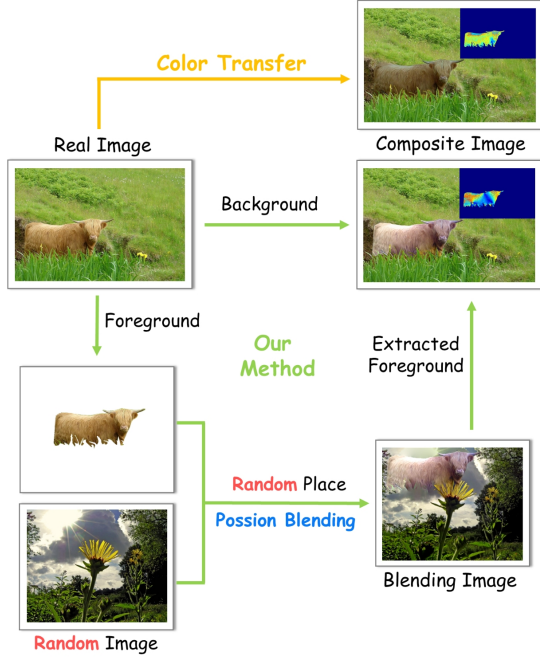


Figure 3. **Random Poisson Blending Process.** The comparison of composite images shows that our method introduces more diverse local variations.

but also pushed away from the negative samples (composite images). The formula is similar to the first term of (Hang et al. 2022), but we use Random Poisson Blending to generate more composite images as negative data.

$$\mathcal{L}_{cr} = \frac{D(f, f^+)}{D(f, f^+) + \sum_{k=1}^K D(f, f^-)} \quad (4)$$

In Eq. (4), f , f^+ , f^- are the feature vectors of the foreground region of the reconstructed image, the GT, and the composite images, respectively. The feature vector is extracted from a pre-trained VGG16 network (Simonyan and Zisserman 2015). $D(\cdot)$ is the ℓ_1 distance function. K is set to 3 as the number of negative samples. The final loss is given by the following equation. To balance the influence of different losses, we empirically set the value of λ to 0.3.

$$\mathcal{L}_{VAE} = \mathcal{L}_{rec} + \lambda \mathcal{L}_{cr} \quad (5)$$

Training of LDM For the learning process of harmonization in latent space, where $z_0, c, \epsilon \sim \mathcal{N}(0, 1)$, the loss is defined as:

$$\mathcal{L}_{LDM} = \frac{M \cdot \|\epsilon - \epsilon_\theta(z_t, t, c)\|_2^2}{\max\{A_{min}, \sum_{h,w} M_{h,w}\}} \quad (6)$$

Eq. (6) can be seen as the implementation of the foreground MSE loss (Sofiuk, Popenova, and Konushin 2020) in the latent space. H , W represent the height and width of the image in the latent space and M is the mask resized to (H, W) . A_{min} is a hyper-parameter. We set $A_{min} = HW/5$ in all our experiments.

Unlike general visual generation, when applying LDM to image harmonization, the generated content is strictly constrained, requiring adjustments to the original style. We found that pretraining the diffusion network specifically for the image harmonization task is necessary.

Therefore, in the first stage, we independently train the U-Net to obtain a diffusion network with image harmonization capabilities. In the second stage, we integrate the Harmony Controller (initialized with the weights of the UNet Encoder), lock the U-Net backbone, and fine-tune it. This stage of the training is similar to ControlNet (Zhang, Rao, and Agrawala 2023).

Dataset Construct

Random Poisson Blending

Color-to-color transformation methods, represented by color transfer, have been widely adopted for synthesized datasets construction (Tsai et al. 2017; Cong et al. 2020). The foregrounds produced by these methods exhibit noticeable global changes but lack local dynamics, which to some extent limits the effectiveness of image harmonization (Ren et al. 2024).

To address the aforementioned limitations, we propose a Region-to-Region transformation method, **Random Poisson Blending**. Specifically, we use Poisson Blending (Pérez, Gangnet, and Blake 2003) to transfer color and light condition from a random region in a random image to the foreground of a real image, creating more diverse and challenging composite images.

As shown in Fig. 3, the process of our method is as follows: (1) Given an image I_t and the foreground mask M , we obtain the foreground object F_t from I_t , where F_t is the foreground that needs to be adjusted. (2) We randomly select a different image I_r from the dataset as the reference image. Then, we randomly choose a region in I_r and apply Poisson blending to blend F_t onto I_r , resulting in I_p . (3) Based on the blending position, we extract the new foreground F_p from I_p . To control the strength of the Poisson blending, we introduce a hyper-parameter α , so that $\tilde{F}_p = \alpha \times F_p + (1 - \alpha) \times F_t$. (4) We paste \tilde{F}_p back into its original position to obtain the synthetic image \tilde{I}_t . To ensure the validity of Poisson Blending and the quality of the synthetic image, we perform some additional operations, the details of which are provided in the Supplementary.

Unlike color transfer based on global color statistics, our approach leverages richer low-level background cues—including color patterns, texture, layout, and lighting—that jointly contribute to disharmony in a semantically agnostic manner.

From the comparison in Fig. 3, it is evident that our method generates composite images with richer local changes, which pose greater challenges for image harmonization. More results generated by our method can be found in the Supplementary Material.

Composite Image Generation and Filtering

We choose the DUTS (Wang et al. 2017) and ADE20K (Zhou et al. 2017) datasets as the base datasets.

Method	HCOCO			HAdobe5k			HFlickr			Hday2night			ALL		
	PSNR↑	MSE↓	fMSE↓	PSNR↑	MSE↓	fMSE↓	PSNR↑	MSE↓	fMSE↓	PSNR↑	MSE↓	fMSE↓	PSNR↑	MSE↓	fMSE↓
Composite	33.94	69.37	996.59	28.16	345.54	2051.61	28.32	264.35	1574.37	34.01	109.65	1409.98	31.63	172.47	1376.42
S ² AM	35.47	41.07	542.06	33.77	63.40	404.62	30.03	143.45	785.65	35.69	50.87	835.06	34.35	59.67	594.67
DoveNet	35.83	36.72	551.01	34.34	52.32	380.39	30.21	133.14	827.03	35.27	51.95	1075.71	34.76	52.33	532.62
RAINNet	37.08	29.52	501.17	36.22	43.35	317.35	31.64	110.59	688.40	34.83	57.40	916.48	36.12	40.29	469.60
iDIH-HRNet	39.64	14.01	N/A	37.35	21.36	N/A	34.03	60.41	N/A	37.68	50.61	N/A	38.31	22.00	252.00
DCCF	39.52	14.87	272.10	37.18	23.43	172.49	33.84	61.42	411.56	38.08	45.09	655.46	38.50	22.05	265.52
PCT-Net	40.78	10.72	208.26	39.97	21.25	157.24	35.13	44.30	341.10	37.65	44.74	654.81	39.85	18.16	216.25
GKNet	40.32	12.95	222.31	39.97	17.94	138.22	34.45	57.58	372.90	38.47	42.76	546.06	39.53	19.90	220.44
HDNet	41.04	11.60	N/A	41.17	13.58	N/A	35.81	47.39	N/A	38.85	31.97	N/A	40.46	16.55	179.49
AICT	40.68	10.74	206.24	40.55	16.50	133.15	35.33	42.58	320.45	37.93	41.27	594.92	39.99	16.53	204.67
DiffHarmony	41.71	9.18	170.44	41.08	19.51	120.78	37.10	30.89	216.27	39.45	22.42	470.846	40.97	14.86	166.48
DiffHarmony++	<u>42.42</u>	<u>8.43</u>	<u>155.73</u>	<u>41.78</u>	18.81	113.18	<u>37.74</u>	<u>28.77</u>	<u>201.52</u>	39.49	<u>22.48</u>	464.35	<u>41.66</u>	13.98	153.98
Ours	42.62	7.93	146.81	42.22	<u>15.70</u>	102.14	38.04	26.28	185.38	39.42	22.64	497.185	41.94	12.51	144.38

Table 1. **Quantitative comparisons across four sub-datasets of iHarmony4 (Cong et al. 2020).** ↑ indicates the higher the better, and ↓ indicates the lower the better. Best results are in bold and the suboptimal results are in underline.

Both of these datasets were originally created for image segmentation tasks and have high-quality masks. They contain 15,572 and 27,574 image pairs, respectively, covering most daily life scenarios. For each real image I_r , our method generates N alternative synthesized versions as candidates $\{\tilde{I}_r^{(i)}\}_{i=1}^N$. We then apply an aesthetic scoring model (Kitada 2022) and manual filtering to remove suboptimal synthesized images.

Since our composite image generation is based on **Random Poisson Blending**, the dataset is named **RPHarmony**, which consists of 12,787 training images and 1,422 test images. Based on the image sources, RPHarmony can be divided into two sub-datasets, namely R-DUTS and R-ADE. Further details on the synthetic datasets are provided in the Supplementary.

Experiments

Datasets and Metrics

We conducted experiments on the iHarmony4 dataset (Cong et al. 2020), comprising four subsets: HCOCO, HAdobe5k, HFlickr, and Hday2night, with 65,742 image pairs for training and 7,404 for testing. Each image pair consists of a synthetic composite image, its foreground mask, and a corresponding real image. Following (Zhou, Feng, and Wang 2024; Zhou et al. 2024), training images were resized to 512×512. Testing was performed on images at a size of 1024×1024, with results subsequently resized to 256×256 for evaluation.

For the experiments on RPHarmony, we first initialized the models with weights pre-trained on iHarmony4 and then finetune the model on RPHarmony. Training and testing configurations were identical to those used for iHarmony4. Performance was evaluated using PSNR, MSE, fMSE, and SSIM.

Implementation Details

The following describes the training configurations for our model on the iHarmony4 dataset. Training details for models involved in the RPHarmony dataset can be found in the Supplementary.

We trained the Clear-VAE model for 30 epochs using the AdamW optimizer with $\beta_1 = 0.9$ and $\beta_2 = 0.999$. The learn-

Model	PSNR↑	MSE↓	fMSE↓	SSIM↑
Composite	25.91	366.32	2362.08	0.9580
PCT-Net	33.26	60.39	332.61	0.9796
AICT	33.28	60.38	333.15	0.9547
HDNet	34.46	47.52	252.54	0.981
DiffHarmony++	<u>36.03</u>	<u>42.16</u>	<u>203.45</u>	<u>0.9861</u>
Ours	36.32	40.25	192.66	0.9872

Table 2. **Quantitative comparisons on RPHarmony.** Best results are in bold and the suboptimal results are in underline.

ing rate of $1e-4$ and the batch size of 4 were used, with gradients accumulated over 8 batches (accumulate_grad_batches = 8). LDM training consists of two stages. In the first stage, we pretrained the U-Net following the experimental setup of DiffHarmony (Zhou, Feng, and Wang 2024). Secondly, the Controller was trained for 5 epochs on the iHarmony4 training set using the AdamW optimizer, with a learning rate of $1e-5$. Data augmentation included random resized crops and random horizontal flips. We set the batch size to 4 with gradient accumulation over 8 batches. Inference employed the Euler ancestral discrete scheduler (Wang, He, and Tao 2024) with 10 sampling steps. Our models were implemented in PyTorch and trained on three NVIDIA 4090 GPUs.

Comparison with Other Methods

We compared our approach against LDM-based models (Zhou, Feng, and Wang 2024; Zhou et al. 2024) and other SOTA methods (Cun and Pun 2020; Cong et al. 2020; Ling et al. 2021; Sofiuk, Popenova, and Konushin 2020; Xue et al. 2022; Guerreiro, Nakazawa, and Stenger 2023; Shen et al. 2023; Chen et al. 2023a; Meng et al. 2024).

Performance comparisons on the iHarmony4. Fig. 1 show our method outperforms existing approaches on almost all metrics across each subset of the test set. Results for other methods were taken from their respective publications or generated using their official code. While our method achieves slightly lower performance on the Hday2night subset, this can likely be attributed to its smaller size and differing image content compared to the other subsets (Guerreiro, Nakazawa, and Stenger 2023). Qualitative results are shown in Fig. 2.

Performance comparisons on the RPHarmony. After

Model	Params	Real Images		Generated Images	
		MSE↓	fMSE↓	MSE↓	fMSE↓
SD-VAE	83.65 M	22.94	678.73	13.51	160.01
Harmony-VAE	+36.1M	1.72	29.66	12.63	147.03
w/o AF	+1.90M	1.52	25.82	12.58	146.76
w/o \mathcal{L}_{cr}	+1.90M	1.78	32.30	12.66	147.13
Ours	+1.90M	1.44	24.68	12.51	144.38

Table 3. **Performance of different VAE design.** Params represents the model’s parameter count, where “+xM” indicates an increase of xM parameters compared to the SD-VAE.

Datset	Variant	PSNR↑	MSE↓	fMSE↓
iHarmony4	w/o Controller	41.76	13.44	149.77
	w/o MACA	41.92	12.55	145.02
	Ours	41.94	12.51	144.38
ccHarmony	w/o Controller	41.54	20.88	168.54
	w/o MACA	41.66	22.07	172.24
	Ours	41.57	20.80	165.99

Table 4. **Quantitative ablation study of our model variants on iHarmony4 (Cong et al. 2020) and ccHarmony (Niu et al. 2023).** The best results are in bold



Figure 4. **Qualitative results on the RealHM (Jiang et al. 2021)** * denotes models that are fine-tuned on the RPHarmony dataset.

fine-tuning on the RPHarmony dataset, we compared our method with recent SOTA models (Guerreiro, Nakazawa, and Stenger 2023; Meng et al. 2024; Chen et al. 2023a; Zhou et al. 2024) (Fig. 2). The increased foreground variation in RPHarmony presents a greater challenge. Interestingly, several models performing comparably on iHarmony4 showed a significant performance drop on RPHarmony. Our method maintained its superior performance. Qualitative comparisons are shown in the Supplementary.

Ablation Study

Evaluation of Clear-VAE. Fig. 3 examines the impact of Adaptive Filter (AF) and different loss functions on reconstruction quality. We compared several VAE models, including variants of our proposed method, evaluating both the reconstruction of real images (at the training resolution of 256×256) and the generation of images from diffusion models (with an input resolution of 1024×1024). The results clearly demonstrate that high-frequency information extracted by the AF contributes to improved visual consistency. Furthermore, the contrastive regulation loss mitigates the influence of disharmonious factors. Removing ei-

Metric	HDNet	HDNet*	Ours	Ours*
Quality Score ↑	3.824	3.877	4.039	4.082

Table 5. **Quantitative results on the RealHM (Jiang et al. 2021).** The quality score is computed based on the DeQA-Score model (You et al. 2025). * denotes models that are fine-tuned on the RPHarmony dataset. Best results are in bold.

ther component degrades performance. Notably, Clear-VAE is lightweight, introducing only about 2% additional parameters compared to SD-VAE.

Evaluation of MACA Module and Harmony Controller. Tab. 4 shows that the Harmony Controller helps align the generative process with the composite input, ensuring semantic consistency and overall performance. The MACA module further improves results, especially on the ccHarmony dataset, by applying mask-aware attention to better handle disharmony region. Together, they enhance harmonization quality and model generalization.

Effect of Fine-tuning on the RPHarmony Dataset. We conduct a comparison between the lightweight model HDNet (Chen et al. 2023a) and our model, evaluating their performance on the RealHM dataset (Jiang et al. 2021) before and after fine-tuning on RPHarmony. Fine-tuned models generalize better to real scenarios, adapting to realistic lighting over simple color alignment, as supported by qualitative results (Fig. 4) and quality score improvements (Tab. 5). More results and details are provided in the Supplementary.

Conclusion

In this work, we introduce the Region-to-Region transformation, which injects information from appropriate regions into the foreground, enabling both better harmonization and the generation of new composite data. Building upon this, we propose R2R, a novel model that incorporates Clear-VAE with Adaptive Filter for preserving high-frequency details and eliminating disharmonious elements, as well as the Harmony Controller with Mask-aware Adaptive Channel Attention (MACA) to dynamically adjust the foreground based on both foreground and background channel importance. To further improve the quality of training data, we propose Random Poisson Blending, a region-to-region transformation method for composite image generation, and construct RPHarmony dataset, which better captures complex real-world lighting conditions. Extensive experiments demonstrate the effectiveness of our method. Additionally, models trained on RPHarmony produce more visually harmonious images in real-world scenarios. Considering the current limitation of model size, future work will explore lightweight diffusion models to improve efficiency. Additionally, we plan to apply Random Poisson Blending to construct larger-scale datasets and investigate the relationship between dataset scale and model generalization.

References

- Cao, J.; Cong, W.; Niu, L.; Zhang, J.; and Zhang, L. 2022. Deep Image Harmonization by Bridging the Reality Gap. *arXiv:2103.17104*.
- Chen, H.; Gu, Z.; Li, Y.; Lan, J.; Meng, C.; Wang, W.; and Li, H. 2023a. Hierarchical Dynamic Image Harmonization. *arXiv:2211.08639*.
- Chen, J.; Zou, Z.; Zhang, Y.; Chen, K.; and Shi, Z. 2023b. Zero-Shot Image Harmonization with Generative Model Prior. *arXiv preprint arXiv:2307.08182*.
- Chen, X.; Huang, L.; Liu, Y.; Shen, Y.; Zhao, D.; and Zhao, H. 2024. AnyDoor: Zero-shot Object-level Image Customization. *arXiv:2307.09481*.
- Cohen-Or, D.; Sorkine, O.; Gal, R.; Leyvand, T.; and Xu, Y.-Q. 2006. Color harmonization. *ACM Trans. Graph.*, 25(3): 624–630.
- Cong, W.; Tao, X.; Niu, L.; Liang, J.; Gao, X.; Sun, Q.; and Zhang, L. 2022. High-Resolution Image Harmonization via Collaborative Dual Transformations. *arXiv:2109.06671*.
- Cong, W.; Zhang, J.; Niu, L.; Liu, L.; Ling, Z.; Li, W.; and Zhang, L. 2020. DoveNet: Deep Image Harmonization via Domain Verification. *arXiv:1911.13239*.
- Cun, X.; and Pun, C.-M. 2020. Improving the Harmony of the Composite Image by Spatial-Separated Attention Module. *IEEE Transactions on Image Processing*, 29: 4759–4771.
- Guerreiro, J. J. A.; Nakazawa, M.; and Stenger, B. 2023. PCT-Net: Full Resolution Image Harmonization Using Pixel-Wise Color Transformations. In *2023 IEEE/CVF Conference on Computer Vision and Pattern Recognition (CVPR)*, 5917–5926.
- Hachnochi, R.; Zhao, M.; Orzech, N.; Gal, R.; Mahdavi-Amiri, A.; Cohen-Or, D.; and Bermanno, A. H. 2023. Cross-domain Compositing with Pretrained Diffusion Models. *arXiv:2302.10167*.
- Hang, Y.; Xia, B.; Yang, W.; and Liao, Q. 2022. SCS-Co: Self-Consistent Style Contrastive Learning for Image Harmonization. *arXiv:2204.13962*.
- Ho, J.; Jain, A.; and Abbeel, P. 2020. Denoising Diffusion Probabilistic Models. *arXiv:2006.11239*.
- Hu, Z.; Nsambi, N. E.; Wang, X.; and Wang, Q. 2024. SID-Net: Learning Shading-Aware Illumination Descriptor for Image Harmonization. *IEEE Transactions on Emerging Topics in Computational Intelligence*, 8(2): 1290–1302.
- Jia, J.; Sun, J.; Tang, C.-K.; and Shum, H.-Y. 2006. Drag-and-drop pasting. *ACM Trans. Graph.*, 25(3): 631–637.
- Jiang, Y.; Zhang, H.; Zhang, J.; Wang, Y.; Lin, Z.; Sunkavalli, K.; Chen, S.; Amirghodsi, S.; Kong, S.; and Wang, Z. 2021. SSH: A Self-Supervised Framework for Image Harmonization. *arXiv:2108.06805*.
- Kitada, S. 2022. Aesthetics-Predictor-V2-SAC-Logos-AVA1-L14-LinearMS. <https://huggingface.co/shunk031/aesthetics-predictor-v2-sac-logos-ava1-l14-linearMSE>.
- Laffont, P.-Y.; Ren, Z.; Tao, X.; Qian, C.; and Hays, J. 2014. Transient attributes for high-level understanding and editing of outdoor scenes. *ACM Trans. Graph.*, 33(4).
- Li, J.; Wang, J.; Wang, C.; and Xiong, J. 2023. Image Harmonization with Diffusion Model. *arXiv:2306.10441*.
- Li, L.; Gong, K.; Li, W.; Dai, X.; Chen, T.; Yuan, X.; and Yue, X. 2024. BIFRÖST: 3D-Aware Image compositing with Language Instructions. In *Advanced Neural Information Processing System (NeurIPS)*.
- Ling, J.; Xue, H.; Song, L.; Xie, R.; and Gu, X. 2021. Region-aware Adaptive Instance Normalization for Image Harmonization. *arXiv:2106.02853*.
- Meng, Q.; Liu, Q.; Li, Z.; Lan, X.; Zhang, S.; and Nie, L. 2024. High-Resolution Image Harmonization with Adaptive-Interval Color Transformation. In *The Thirty-eighth Annual Conference on Neural Information Processing Systems*.
- Niu, L.; Cong, W.; Liu, L.; Hong, Y.; Zhang, B.; Liang, J.; and Zhang, L. 2024. Making Images Real Again: A Comprehensive Survey on Deep Image Composition. *arXiv:2106.14490*.
- Niu, L.; Tan, L.; Tao, X.; Cao, J.; Guo, F.; Long, T.; and Zhang, L. 2023. Deep Image Harmonization with Globally Guided Feature Transformation and Relation Distillation. *arXiv:2308.00356*.
- Pérez, P.; Gangnet, M.; and Blake, A. 2003. Poisson image editing. *ACM Trans. Graph.*, 22(3): 313–318.
- Pitie, F.; Kokaram, A.; and Dahyot, R. 2005. N-dimensional probability density function transfer and its application to color transfer. In *Tenth IEEE International Conference on Computer Vision (ICCV'05) Volume 1*, volume 2, 1434–1439 Vol. 2.
- Ren, M.; Xiong, W.; Yoon, J. S.; Shu, Z.; Zhang, J.; Jung, H.; Gerig, G.; and Zhang, H. 2024. Relightful Harmonization: Lighting-aware Portrait Background Replacement. *arXiv:2312.06886*.
- Rombach, R.; Blattmann, A.; Lorenz, D.; Esser, P.; and Ommer, B. 2022. High-Resolution Image Synthesis with Latent Diffusion Models. *arXiv:2112.10752*.
- Shen, X.; Zhang, J.; Chen, J.; Bai, S.; Han, Y.; Wang, Y.; Wang, C.; and Liu, Y. 2023. Learning Global-aware Kernel for Image Harmonization. *arXiv:2305.11676*.
- Simonyan, K.; and Zisserman, A. 2015. Very Deep Convolutional Networks for Large-Scale Image Recognition. *arXiv:1409.1556*.
- Sofiuk, K.; Popenova, P.; and Konushin, A. 2020. Foreground-aware Semantic Representations for Image Harmonization. *arXiv:2006.00809*.
- Song, J.; Meng, C.; and Ermon, S. 2022. Denoising Diffusion Implicit Models. *arXiv:2010.02502*.
- Song, S.; Zhong, F.; Qin, X.; and Tu, C. 2020. Illumination Harmonization with Gray Mean Scale. In Magnenat-Thalmann, N.; Stephanidis, C.; Wu, E.; Thalmann, D.; Sheng, B.; Kim, J.; Papagiannakis, G.; and Gavrilova, M., eds., *Advances in Computer Graphics*, 193–205. Cham: Springer International Publishing. ISBN 978-3-030-61864-3.

- Tsai, Y.-H.; Shen, X.; Lin, Z.; Sunkavalli, K.; Lu, X.; and Yang, M.-H. 2017. Deep Image Harmonization. arXiv:1703.00069.
- Wang, L.; Lu, H.; Wang, Y.; Feng, M.; Wang, D.; Yin, B.; and Ruan, X. 2017. Learning to Detect Salient Objects with Image-level Supervision. In *CVPR*.
- Wang, Y.; He, Y.; and Tao, M. 2024. Evaluating the design space of diffusion-based generative models. arXiv:2406.12839.
- Woo, S.; Park, J.; Lee, J.-Y.; and Kweon, I. S. 2018. CBAM: Convolutional Block Attention Module. In Ferrari, V.; Hebert, M.; Sminchisescu, C.; and Weiss, Y., eds., *Computer Vision – ECCV 2018*, 3–19. Cham: Springer International Publishing. ISBN 978-3-030-01234-2.
- Xue, B.; Ran, S.; Chen, Q.; Jia, R.; Zhao, B.; and Tang, X. 2022. DCCF: Deep Comprehensible Color Filter Learning Framework for High-Resolution Image Harmonization. arXiv:2207.04788.
- You, Z.; Cai, X.; Gu, J.; Xue, T.; and Dong, C. 2025. Teaching Large Language Models to Regress Accurate Image Quality Scores using Score Distribution. In *IEEE Conference on Computer Vision and Pattern Recognition*.
- Yu, Y.; Zeng, Z.; Hua, H.; Fu, J.; and Luo, J. 2024. Prompt-Fix: You Prompt and We Fix the Photo. arXiv:2405.16785.
- Zhang, L.; Rao, A.; and Agrawala, M. 2023. Adding Conditional Control to Text-to-Image Diffusion Models. arXiv:2302.05543.
- Zhou, B.; Zhao, H.; Puig, X.; Fidler, S.; Barriuso, A.; and Torralba, A. 2017. Scene Parsing through ADE20K Dataset. In *Proceedings of the IEEE Conference on Computer Vision and Pattern Recognition*.
- Zhou, P.; Feng, F.; Liu, G.; Li, R.; and Wang, X. 2024. DiffHarmony++: Enhancing Image Harmonization with Harmony-VAE and Inverse Harmonization Model. In *ACM MM*.
- Zhou, P.; Feng, F.; and Wang, X. 2024. DiffHarmony: Latent Diffusion Model Meets Image Harmonization. In *Proceedings of the 2024 International Conference on Multimedia Retrieval*, 1130–1134.